universe

MDPI

Communication

Highlight Talk from Super-Kamiokande †

Yuuki Nakano and on behalf of the Super-Kamiokande Collaboration

Kamioka Observatory, Institute for Cosmic Ray Research, The University of Tokyo, Higashi-Mozumi 456, Kamioka-cho, Hida-city Gifu 506-1205, Japan; ynakano@km.icrr.u-tokyo.ac.jp; Tel.: +81-578-85-9665

† This paper is based on the talk at the 7th International Conference on New Frontiers in Physics (ICNFP 2018), Crete, Greece, 4–12 July 2018.

Received: 30 November 2018; Accepted: 7 January 2019; Published: 9 January 2019

check for updates

Abstract: Super-Kamiokande (SK), a 50 kton water Cherenkov detector in Japan, is observing both atmospheric and solar neutrinos. It is also searching for supernova (relic) neutrinos, proton decays and dark matter-like particles. A three-flavor oscillation analysis was conducted with the atmospheric neutrino data to study the mass hierarchy, the leptonic CP violation term, and other oscillation parameters. In addition, the observation of solar neutrinos gives precise measurements of the energy spectrum and oscillation parameters. In this proceedings, we given an overview of the latest results from SK and the prospect toward the future project of SK-Gd.

Keywords: Super-Kamiokande; atmospheric neutrino; solar neutrino; neutrino oscillation; CP violation; proton decay

1. Introduction

A theoretical framework of neutrino oscillation has been established in the past 50 years [1,2]. Neutrino physics has been dominated by the measurement of oscillation parameters and such measurements suggest that neutrinos are massive and mixing in the lepton sector [3]. Within the three-flavor framework, three mixing angles (θ_{12}, θ_{23}, *and* θ_{13}) and two mass splittings (Δm^2_{21} *and* $\Delta m^2_{32,31}$) are measured among neutrino experiments.

However, more precise measurements are required to reveal CP violation phase and neutrino mass hierarchy. In addition, another interest is the change of the probability of neutrino oscillation when neutrinos pass through matter [4,5]. To address these unknown properties of neutrinos, any difference between neutrino and anti-neutrino should be tested among neutrino experiments.

2. Super-Kamiokande Detector

The Super-Kamiokande (SK) is a water Cherenkov detector located at 1000 m (2700 m water equivalent) below the top of Mt. Ikenoyama in Gifu prefecture, Japan [6]. It is a cylindrical stainless tank structure and contains 50 ktons of ultra pure water. (The resistivity of the purified water is close to the chemical limit of 18.07 MΩ·cm. Because of its high purity, the water transparency for light in water in the tank is longer than 100 m.) The detector is divided into two regions by the detector structure to separate themselves optically with Tyvek sheet [7]: one is the inner detector (ID) and the other is the outer detector (OD). The ID serves as the target of interactions and the OD is used to veto external cosmic ray muon. In the ID detector, the diameter (height) of the cylindrical tank is 33.8 m (36.2 m). It contains 32 kton of water and holds 11,129 inward-facing 20-inch photomultipliers (PMTs) [8] to observe the Cherenkov light produced by penetrating charged particles. On the other hand, the diameter (height) of the OD tank is 39.3 m (41.4 m). It holds 1885 outward-facing 8-inch PMTs to detect cosmic ray muons in the OD. The configuration of detector and performance is described in Refs. [6,7].

The first phase of the SK experiment (SK-I) began with the original configuration in April 1996. The latter phases are described in Table 1. On May 2018, the fourth phase of SK (SK-IV) ended physics data collection to refurbish the detector toward the next project of SK (SK-Gd) described in Section 5.

Table 1. Experimental phases of Super-Kamiokande detector. For the energy threshold, the recoil electron kinetic energy is shown.

Phase	SK-I	SK-II	SK-III	SK-IV
Period	April 1996–July 2001	October 2002–October 2005	July 2006–August 2008	September 2008–May 2018
ID PMTs [8]	11,149	5182	11,129	11,129
OD PMTs	1885	791	1885	1885
Photo coverage	40%	19%	40%	40%
Energy threshold	4.5 MeV	6.5 MeV	4.0 MeV	3.5 MeV
Electronics	ATM [9,10]	ATM	ATM	Qbee [11,12]

The ring pattern of the observed Cherenkov light produced by charged particles enables the detector to reconstruct the initial interaction vertex and the energy. With this water Cherenkov technique, SK can study many interactions between neutrinos and nucleus as well as proton decay in the energy range from a few MeV to tens of GeV. Therefore, SK is a multi-purpose detector with rich physics targets. SK has obtained many physics results, such as atmospheric neutrino [13–15], solar neutrino [16,17], supernova (relic) neutrino [18], proton decay [19,20], dark matter-like particle (for example, weakly interacting massive particles (WIMPs) [21–24], neutralino [25–27] and boosted dark matter [28–30]) [31,32] and other exotic physics beyond the standard model [33,34]. The publications from the SK collaboration are summarized in Ref. [35].

In this proceedings, the results described in Ref. [14,15] as well as the updated results of Ref. [17] are briefly discussed. In addition, the future upgrade of the SK detector is also described.

3. Atmospheric Neutrino

3.1. Introduction

Atmospheric neutrinos are produced by interactions of primary cosmic rays with nuclei in upper atmosphere. They mainly consist of ν_e and ν_μ produced from the decays of charged mesons and muons and travel 10–13,000 km depending on the production point. Atmospheric neutrino oscillations are mainly described as the oscillation of $\nu_\mu \to \nu_\tau$, which depends on the mixing angle θ_{23} and the mass splitting $\Delta m^2_{32,31}$. Because the pattern of neutrino oscillations depends on the ratio of the travel length and the energy of neutrino (L/E), atmospheric neutrinos are an excellent tool for studies of neutrino oscillation. Their flux and energy distribution are well modeled [36–39] and are precisely measured by SK at Kamioka experimental site [13].

In particular, upward-going electron neutrinos passing through the earth give important information of neutrino properties because the resonant enhancement of the $\nu_\mu \to \nu_e$ oscillation probability in multi-GeV region is expected due to the effect of θ_{13} and earth's matter [40–42]. The resonance occurs only for electron neutrinos (anti-neutrinos) when the mass hierarchy is normal (inverted). In the same energy region, θ_{23} octant also affects the amplitude of the resonance. In the sub-GeV region, the CP value affects the absolute flux of electron neutrinos [43].

3.2. Three-Flavor Oscillation Analysis

A study of the neutrino oscillation parameters ($\sin^2\theta_{23}$, Δm^2_{32}, δ_{CP} and mass hierarchy) was performed using 5326 days of atmospheric neutrino data taken from SK-I to SK-IV. In the high energy region above 100 MeV, the neutrino events are categorized into three types, namely fully contained (FC), partially contained (PC) and upward-going muon (UPMU), based on the event topology. In addition, the atmospheric neutrino samples are divided into sub-groups, based on for example the energy range (sub-GeV and multi-GeV), e-like or μ-like of events and the number of Cherenkov rings. In particular, multi-GeV and e-like samples are further divided into neutrino-like and anti-neutrino-like samples to obtain sensitivity to the mass hierarchy. Finally, the atmospheric neutrino samples are divided into 19 samples in total. Figure 1a shows the momentum distribution and zenith angle distribution of atmospheric neutrino samples.

Figure 1b shows the constraints on the neutrino nixing parameters from SK atmospheric neutrino data assuming $\sin^2\theta_{13} = 0.0219 \pm 0.0012$ [44] according to the short baseline reactor measurements. The obtained values in this analysis are summarized in Table 2. The oscillation values are in good agreement with other experiments, such as T2K, NOvA, IceCube and MINOS [45–49]. Based on the minimum value of χ^2, the SK data prefer the normal hierarchy over the inverted hierarchy with $\Delta\chi^2 = \chi^2_{\text{Normal, min}} - \chi^2_{\text{Inverted, min}} = -4.33$.

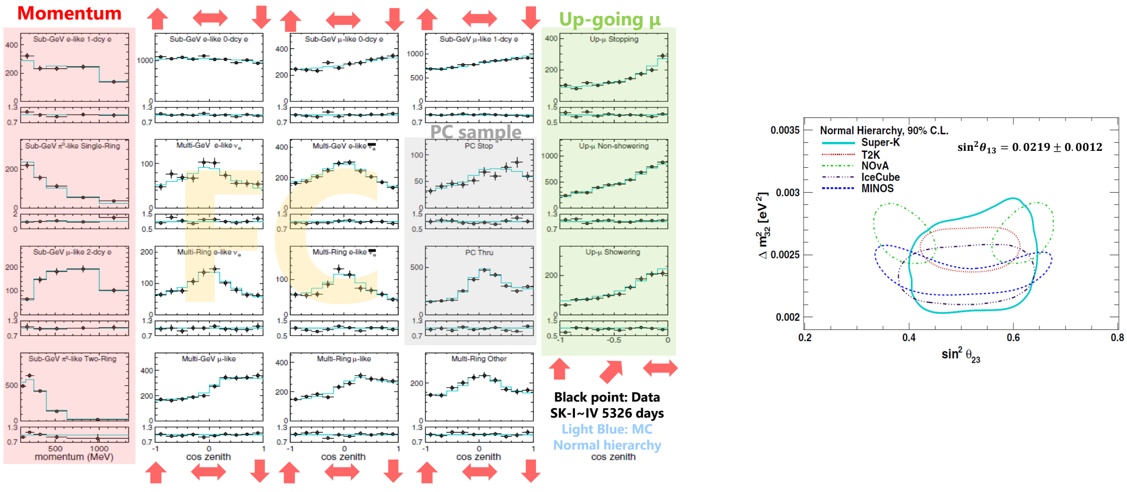

Figure 1. (**a**) Data and MC comparison for the entire SK data divided into 19 analysis samples. (**b**) The 90% C.L. constraint of oscillation parameters using SK atmospheric data together with other experiments (T2K [46], NovA [47], IceCube [48] and MiNOS [49]) assuming the normal hierarchy. The original figures are adapted from Ref. [14].

Table 2. Result of oscillation analysis from atmospheric neutrino data taken in SK assuming $\sin^2\theta_{13} = 0.0219 \pm 0.0012$ [44].

Mass Hierarchy	χ^2	$\lvert\Delta m^2_{32,31}\rvert$ [$\times 10^{-3}$ eV^2]	$\sin^2\theta_{23}$	δ_{CP}
Normal hierarchy	571.33	$2.50^{+0.13}_{-0.20}$	$0.588^{+0.031}_{-0.064}$	$4.18^{+1.41}_{-1.61}$
Inverted hierarchy	575.66	$2.50^{+0.08}_{-0.37}$	$0.575^{+0.036}_{-0.073}$	$4.18^{+1.52}_{-1.66}$

As shown in Figure 1b, T2K's measurements of $\sin^2\theta_{23}$, and Δm^2_{32} are more constraining than those of SK [45,46]. Therefore, an external constraint with T2K experiment enhances the sensitivity of this analysis when combining with the atmospheric neutrino data in SK. Figure 2 shows the constraint on the neutrino parameters from a combined fit with SK atmospheric neutrino data with T2K public data.

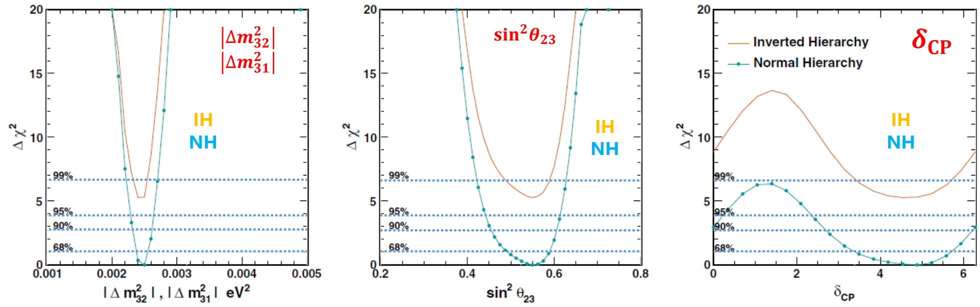

Figure 2. The constraint on the neutrino parameters from a combined fit with SK atmospheric neutrino data and the model of T2K experiment assuming $\sin^2\theta_{13} = 0.0219 \pm 0.0012$ [44]. The original figure is adapted from Ref. [14].

The obtained values with the T2K constraints are summarized in Table 3. Based on the minimum value of χ^2, the SK plus T2K data prefer the normal hierarchy over the inverted hierarchy with $\Delta\chi^2 = \chi^2_{\text{Normal, min}} - \chi^2_{\text{Inverted, min}} = -5.27$.

Table 3. Result of oscillation analysis combined with T2K public data [45,46].

Mass Hierarchy	χ^2	$\lvert\Delta m^2_{32,31}\rvert$ [$\times 10^{-3}$ eV^2]	$\sin^2\theta_{23}$	δ_{CP}
Normal hierarchy	639.43	$2.50^{+0.05}_{-0.12}$	$0.550^{+0.039}_{-0.057}$	$4.88^{+0.81}_{-1.48}$
Inverted hierarchy	644.70	$2.40^{+0.13}_{-0.06}$	$0.550^{+0.035}_{-0.051}$	$4.54^{+1.05}_{-0.97}$

3.3. Tau Neutrino Appearance

In the framework of three-flavor neutrino oscillation, neutrinos produced in a specific lepton flavor can change to a different flavor during their travel. In the upward neutrinos, ν_μ can travel enough to oscillate to ν_τ while the intrinsic ν_τ in the atmospheric neutrino flux are negligible because of its small production rate [50].

To search for ν_τ appearance in the atmospheric neutrinos, the charged current reaction (CC) of ν_τ in SK have been searched. The CC ν_τ reaction produces single tau lepton in the water. Then, tau lepton decays into secondary particles soon after its production because of short life-time. Finally, cascade-like events (with many Cherenkov rings) are detected in the SK detector. The cross-section of ν_τ is greatly suppressed because the τ lepton has large mass relative to electron and muon at the low energy. Therefore, the search for ν_τ in the SK has an energy threshold of 3.5 GeV.

To predict the rate of both CC tau interaction and atmospheric neutrino background, MC simulation is used based on the neutrino interaction model as well as the detector response of SK. SK performed a search for CC-event due to ν_τ with a neural network algorithm developed in Ref. [51]. The selection efficiencies for this analysis are 86% for the ν_τ CC event and 23% for the background of other atmospheric neutrino events. Although it is hard to identify ν_τ CC reaction by reaction in this analysis, CC ν_τ event can be statistically found over background in the up-going sample. The analysis was performed using two-dimensional unbinned maximum likelihood fit to the observed data including systematic uncertainties:

$$Data = PDF_{\text{BG}} + \alpha \times PDF_{\text{Tau}} + \sum \varepsilon_i \times PDF_i \tag{1}$$

where PDF_{Tau} (PDF_{BG}) is a probability density function for τ-like (background), α is a scaling parameter (no τ contribution when $\alpha = 0$ while MC expected when $\alpha = 1$), ε_i is a magnitude of ith systematic uncertainty and PDF_i is a probability density function for ith systematic uncertainty. Figure 3a shows the zenith angle distribution of τ-like events overlaid with the MC prediction without the τ contribution. A clear excess, 338.1 ± 72.7 events, is observed over the background in the up-going bins (gray in Figure 3a).

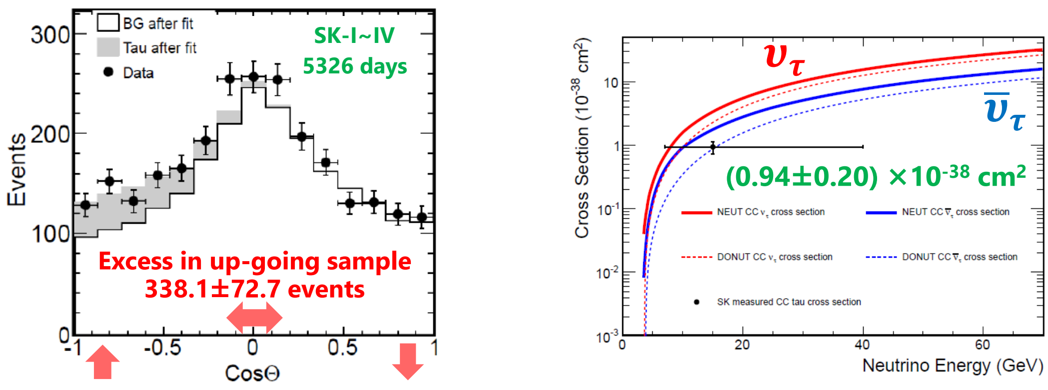

(**a**) (**b**)

Figure 3. (**a**) The zenith angle distribution of the τ-like events. The tau signal drawn in gray is clearly seen over the background in up-going event. (**b**) The cross-section of ν_τ CC measured by this analysis. The original figures are adapted from Ref. [15].

Assuming the normal hierarchy, the value of parameter α is 1.47 ± 0.32 (stat.+syst.), excluding the hypothesis of no-τ-appearance at a significance of 4.6σ. Among neutrino experiments, the cross-section of CC ν_τ has been measured by DONUT, SK and OPERA [15,51–53] while the cross-section of both neutral current (NC) and CC has been measured by IceCube [54]. (Comparison of the parameter α among OPERA, SK and IceCube is discussed in Ref. [54]. Currently, they are consistent with the standard neutrino oscillation framework within their uncertainties.)

Based on the atmospheric neutrino flux model [39] and the observed events, the cross-section of the CC reaction is measured as $(0.94 \pm 0.20) \times 10^{-38}$ cm^2 between 3.5 GeV and 70 GeV, as shown in Figure 3b. This result is consistent with the standard model within 1.5σ.

4. Solar Neutrino

4.1. Introduction

Solar neutrinos are produced by the nuclear fusion reaction, $4p \to \alpha + 2e^+ + 2\nu_e$, in the core of the sun. Electron neutrinos (ν_e) produced in the sun are so-called *pp*, *pep*, ^{7}Be, ^{8}B and *hep* neutrinos as well as *CNO* neutrinos. Their fluxes are well predicted by the standard solar model [55] and are measured by several techniques, such as radiochemical (Homestake [56], SAGE and Gallex/GNO [57]), water Cherenkov (Kamiokande [58], SK and SNO [59]) and liquid scintillator (Borexino [60] and KamLAND [61]).

Solar neutrino flux measurements from Super-Kamiokande (SK) [62] and the Sudbury Neutrino Observatory (SNO) [63] have provided direct evidence for solar neutrino flavor conversion. However, there is still no clear evidence that this solar neutrino flavor conversion is indeed due to neutrino oscillations alone [64]. Several models, which are combinations of the neutrino oscillation plus the physics beyond the standard model, have been proposed to demonstrate the current experiment data, for example sterile neutrinos [65,66], mass-varying neutrino [67] and non-standard interaction [68,69].

One of interesting physics motivations among solar neutrino experiments is to search for the matter effect, which is the so-called Mikheyev–Smirnov–Wolfenstein (MSW) effect [4,5]. The MSW effect leads to a resonant conversion of the higher energy solar neutrinos (especially ^{8}B) within the sun and results in an about 30% level of the survival probability above a few MeV (Up-turn).

SK searches for the "Spectrum up-turn" by measuring the recoil electron energy spectrum since the recoil electron energy spectrum reflects the survival probability of the electron neutrinos. To precisely test the MSW effect in the energy spectrum, several calibration source (or devices) have been used in SK. For example, the electron LINAC [70], which generates electron with uniform energy, and the deuterium-tritium neutron generator, which generates ^{16}N radioisotopes [71], are used to determine the energy scale and both energy and angle resolution. In addition, Ni-Cf calibration source [7] is used to estimate the resolution of the reconstructed position and the detection efficiency of the low energy neutrino-like event. Due to those calibrations, the systematic uncertainty on the ^{8}B solar neutrino flux measurement has achieved at $\pm 1.7\%$ in SK-IV.

In 2016, the Super-Kamiokande collaboration released a paper about the solar neutrino analysis results [17]. In this proceedings, the updated results, except for the day/night flux asymmetry measurement [16], are presented using data taken through the end of December 2017 (SK-IV 2860-day dataset). The total lifetime throughout the different phases of SK [72–74] is 5695 days.

4.2. Flux Measurement

The SK detector observes solar neutrinos via the elastic scattering between the solar neutrinos and the electron in pure water. In the case of ν–e interaction, the direction of the recoil electron is highly correlated with the direction of the incident neutrinos. Figure 4a shows the distribution of cosine between the reconstructed direction of observed recoil electrons and the direction of the sun. Using 2860 days of data in SK-IV, $55,729^{+363}_{-361}$ (stat.) events are observed over the background. Adding the solar neutrino events observed in other phases, the total number of the solar neutrino events reaches about 90,000 events thus far. Based on these data, the ^{8}B solar neutrino flux is determined to be $(2.33 \pm 0.04) \times 10^6/\mathrm{cm}^2/\mathrm{s}$ assuming a pure electron neutrino flavor content. The ratio between the SK result and the SNO NC flux ($5.25 \times 10^6/\mathrm{cm}^2/\mathrm{s}$) [75] becomes 0.4432 ± 0.0084.

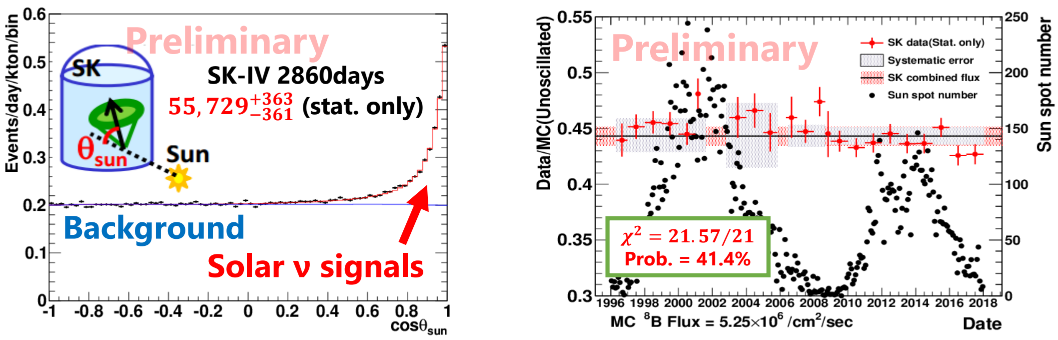

(**a**) (**b**)

Figure 4. (**a**) Distribution of cosine between the direction of the Sun and the reconstructed direction of recoil electrons. (**b**) Solar neutrino event rates relative to the prediction [75] as a function of the time (red points) together with the number of sunspots (black points) [76].

Since the SK has observed solar neutrinos for more than 20 years, this long term observation covers nearly two solar activity cycles. Figure 4b shows the SK yearly flux measured throughout the different phases of SK together with the corresponding sun spot number [76]. Using the present data, the χ^2 is calculated with the total experimental uncertainties as $\chi^2 = 21.57/21$, where 21 is the degree of freedom for χ^2. This corresponds to a probability of 41.4%. The solar rate measurements in SK are fully consistent with a constant solar neutrino flux emitted by the sun.

4.3. Energy Spectrum Analysis

Because of several efforts to reduce background in the SK water (induced by radioisotopes in pure water, especially ^{214}Bi) [77,78], SK-IV has achieved the lowest background among all SK phases. Finally, the energy threshold in SK-IV have been lowered at 3.5 MeV in recoil energy kinetic energy (SK-I: 4.5 MeV, SK-III: 4.0 MeV) and this enables SK to measure the solar neutrino energy spectrum with high sensitivity. In addition, on May 2015, the trigger threshold was changed from 34 observed PMT signals within 200 nsec to 31 hits [12,79]. With this lower threshold, the detection efficiency between 3.5 MeV and 4.0 MeV is improved from $\sim$86% to $\sim$100%. This improvement leads the further reduction of the statistics uncertainty below 5 MeV in SK-IV.

Although an energy of the incident neutrinos is not directly measured in the SK detector, the neutrino energy spectrum can be extracted from the recoil electron energy spectrum in SK. The energy spectrum of recoil electrons are extracted using an extended maximum likelihood fit [72].

The number of expected solar neutrino interactions without the neutrino oscillations is estimated by using the MC simulation considering the cross-section of the ν-e elastic scattering, recoil electron kinematics, the response of the SK detector (PMT and electronics) and the performance of the SK detector (energy scale, energy resolution and so on). After the MC production above, the number of the observed solar neutrino interactions is compared with the expected number of events, thus the survival probability of the electron neutrinos produced in the sun is obtained.

Figure 5a shows the combined energy spectrum from SK-I to SK-IV with the predictions of the MSW effect assuming the current oscillation parameters described below. It is noted that all SK phases are combined without regard to energy resolution or systematic uncertainties in Figure 5a, but those uncertainties are taken into account in the χ^2 calculation between the data and the prediction. Comparing χ^2 between the data (black) and the predictions (green or blue), the energy spectrum of SK is consistent within $\sim$1.2σ with the MSW up-turn for the solar global best-fit parameters (green in Figure 5b) while it disfavors $\sim$2σ with the MSW up-turn for KamLAND best-fit parameters (blue in Figure 5b).

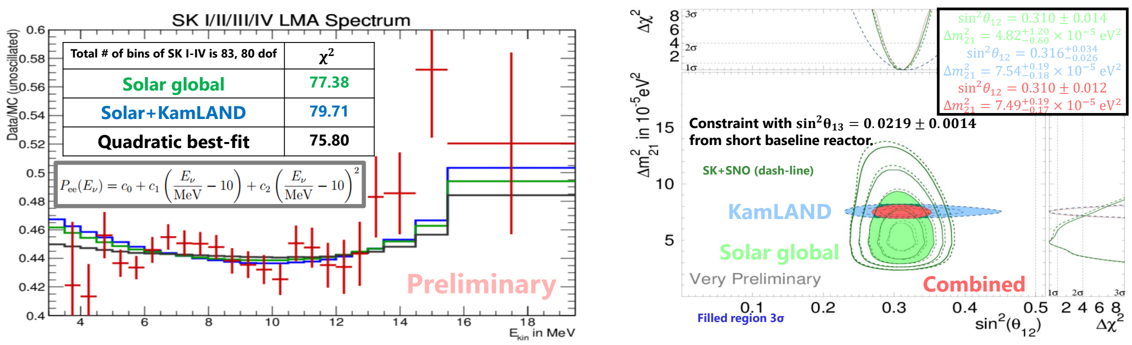

(a) (b)

Figure 5. (**a**) The energy spectrum of recoil electrons from SK-I to SK-IV relative to the SNO NC flux (red point). The expected spectrum assuming the neutrino oscillation with the MSW (green, global solar best-fit parameters; blue, global plus KamLAND parameters). The black spectrum shows the quadratic fitting-function introduced in Ref. [75]. (**b**) Allowed region of oscillation parameters of Δm^2_{21} and $\sin^2\theta_{12}$.

4.4. Neutrino Oscillation Analysis

The oscillation analysis is performed using the results from SK [17,72–74], SNO [75], radiochemical solar neutrino experiments [56,57] and Borexino [80] as well as the anti-neutrino measurement by KamLAND [81]. Based on the measurement from short baseline reactor experiments [82–84], $\sin^2\theta_{13} = 0.0219 \pm 0.0014$ is assumed in this analysis. When combining with results from the other solar neutrino experiments, the mixing angle is determined to be $\sin^2\theta_{12} = 0.310 \pm 0.014$ and the mass difference is determined to be $\Delta m^2_{21} = 4.82^{+1.20}_{-0.60} \times 10^{-5}$ eV^2, as shown in Figure 5b. Adding the KamLAND result, the oscillation parameters are determined as $\sin^2\theta_{12} = 0.310 \pm 0.012$, $\Delta m^2_{21} = 7.49^{+0.19}_{-0.17} \times 10^{-5}$ eV^2. The SK spectrum and day/night data favors a lower Δm^2_{21} value than that measured by KamLAND by more than $\sim$2σ. Further precise measurements are required to confirm this tension in future.

5. Future Prospect (SK-Gd)

5.1. Physics Motivation

Diffused supernova neutrinos (relic neutrinos) are produced by past explosions in the universe. The galactic formation rate can be understood when the production rate of relic neutrinos is known.

Since the cross-section of the inverse beta decay reaction (IBD) between anti-electron neutrino and proton ($\bar{\nu}_e + p \rightarrow e^+ + n$) is relatively large below 100 MeV, there is a chance to search for relic neutrinos between 10 MeV and 30 MeV over backgrounds of reactor, solar and atmospheric neutrinos [85,86]. SK has measured the flux of relic neutrinos with the observed energy spectrum [87] as well as the delayed coincidence technique of neutron tagging on proton [18]. However, the current limit of flux is one order of magnitude higher than some of the theoretical models because the delayed signal of 2.2 MeV gamma ray from neutron capture on proton is difficult to detect in the current SK, where the detection efficiency of neutron tagging is only ∼18% [18,88].

To enhance the sensitivity to relic neutrinos, further reduction of background is required. For this purpose, adding 0.2% of gadolinium sulfate ($Gd_2(SO_4)_3$) into the 50 kton of water tank enables the SK detector to tag neutron produced by the IBD with high efficiency [89]. Since Gd has larger cross-section for thermal neutrino than proton (five orders of magnitude) and emits ∼8 MeV of gamma rays, the detection efficiency for the IBD of $\bar{\nu}_e$ is dramatically improved to be 90% level after adding Gd into SK (SK-Gd).

5.2. Tank Refurbish Work and Future Plan

On 30 May 2018, SK stopped taking physics data to start the tank refurbishment work toward SK-Gd. This refurbishment work aims to replace broken PMTs in both ID and OD, to newly install the water piping line of the new water system for SK-Gd, and to stop water leak from the water tank by sealing the stainless tank wall.

The current plan for the implementation of SK-Gd has three steps. The first is the tank refurbishment, filling water into the tank and then the recirculation of water until the water transparency achieves a good quality. The second is loading $Gd_2(So_4)_3$ up to 0.02% level, where the neutron tagging efficiency on Gd achieves about 50%. Under this condition, we will evaluate the performance of the detector and estimate the background level. The third is loading $Gd_2(So_4)_3$ up to 0.2% level, where the efficiency finally achieves a 90% level. It is noted that the detector performance for neutron tagging is evaluated with a special calibration by putting an apparatus of Am/Be-incorporated BGO crystal into the water tank [88]. Based on the calibration result and MC simulation considering Gd-doped water, the detection efficiency of the neutron tagging in SK with Gd is estimated.

6. Conclusions

Super-Kamiokande is a multi-purpose detector with rich physics targets using the water Cherenkov technique. We measured the neutrino oscillation parameters as well as δ_{CP} using atmospheric neutrinos with the external constraint of T2K data. The SK+T2K data prefer the normal hierarchy over the inverted hierarchy with $\Delta\chi^2 = -5.27$. An analysis searching for the appearance of ν_τ in an atmospheric neutrino sample was conducted. The significance of 4.6σ was observed assuming the normal hierarchy.

Due to the large statistics of solar neutrino observation in SK, precise measurements of the solar neutrino flux and the energy spectrum were made. No significant correlation between the ^{8}B solar neutrino flux and the sunspot number was observed. No distortion of the energy spectrum has been observed yet. The value of Δm^2_{21} obtained from the SK solar neutrino data combined with the other solar neutrino experiments has a tension with that from KamLAND reactor neutrino measurements by about 2σ.

To detect supernova relic neutrinos, we are planning to dissolve gadolinium in the SK's water tank to enhance the tagging efficiency of neutrino produced via the inverse beta decay between the anti-electron neutrino and the proton in water. The refurbish works toward SK-Gd started on 30 May 2018.

Author Contributions: These authors contributed equally to this work.

Funding: This work was supported by JSPS KAKENHI, Grant-in-Aid for Young Scientific Research (B) with Grant Number 17K17880 (Y.N.). We gratefully acknowledge cooperation of the Kamioka Mining and Smelting Company. The Super-Kamiokande experiment was built and has been operated with funding from the Japanese Ministry of Education, Science, Sports and Culture, and the U.S. Department of Energy.

Acknowledgments: We gratefully acknowledge the cooperation of the Kamioka Mining and Smelting Company.

Conflicts of Interest: The authors declare no conflict of interest.

References

1. Ziro, M.; Masami, N.; Sakata, S. Remarks on the Unified Model of Elementary Particles. *Prog. Theor. Phys.* **1962**, *28*, 870–880.
2. Pontecorvo, B. Neutrino experiments and the problem of conservation of leptonic. *Sov. Phys. JETP* **1968**, *26*, 984–988.
3. Fukuda, Y.; et al. [Super-Kamiokande Collaboration]. Evidence for Oscillation of Atmospheric Neutrinos. *Phys. Rev. Lett.* **1998**, *81*, 1562. [CrossRef]
4. Mikheyev, S.P.; Smirnov, A.Y. Resonance Amplification of Oscillations in Matter and Spectroscopy of Solar Neutrinos. *Sov. J. Nucl. Phys.* **1985**, *42*, 913–917.
5. Wolfenstein, L. Neutrino oscillations in matter. *Phys. Rev. D* **1978**, *17*, 2369. [CrossRef]
6. Fukuda, S.; et al. [Super-Kamiokande Collaboration]. The Super-Kamiokande detector. *Nucl. Instrum. Methods A* **2003**, *501*, 418–462. [CrossRef]
7. Abe, K.; et al. [Super-Kamiokande Collaboration]. Calibration of the Super-Kamiokande detector. *Nucl. Instrum. Methods A* **2014**, *737*, 253–272. [CrossRef]
8. Kume, H.; Sawaki, S.; Ito, M.; Arisaka, K.; Suzuki, A. 20 inch diameter photomultiplier. *Nucl. Instrum. Methods A* **1983**, *205*, 443–449. [CrossRef]
9. Tanimori, T.; Ikeda, H.; Mori, M.; Kihara, K.; Kitagawa, H.; Haren, Y. Design and performance of semi-custom analog IC including two TACs and two current integrators for 'Super-Kamiokande'. *IEEE Trans. Nucl. Sci.* **1989**, *36*, 497–501. [CrossRef]
10. Ikeda, H.; Ikeda, M.; Inaba, S.; Takasaki, F. Monolithic shaper amplifier for multianode PMT readout. *Nucl. Instrum. Methods A* **1990**, *292*, 439–444. [CrossRef]
11. Nishino, H.; Awai, K.; Hayato, Y.; Nakayama, S.; Okumura, K.; Shiozawa, M.; Takeda, A.; Ishikawa, K.; Minegishi, A.; Arai, Y. High-speed charge-to-time converter ASIC for the Super-Kamiokande detector. *Nucl. Instrum. Methods A* **2009**, *610*, 710–717. [CrossRef]
12. Yamada, S.; Awai, K.; Hayato, Y.; Kaneyuki, K.; Kouzuma, Y.; Nakayama, S.; Nishino, H.; Okumura, K.; Obayashi, Y.; Shimizu, Y.; et al. Commissioning of the New Electronics and Online System for the Super-Kamiokande Experiment. *IEEE Trans. Nucl. Sci.* **2010**, *57*, 428–432. [CrossRef]
13. Richard, E.; et al. [Super-Kamiokande Collaboration]. Measurements of the atmospheric neutrino flux by Super-Kamiokande: Energy spectra, geomagnetic effects, and solar modulation. *Phys. Rev. D* **2016**, *94*, 052001. [CrossRef]
14. Abe, K.; et al. [Super-Kamiokande Collaboration]. Atmospheric neutrino oscillation analysis with external constraints in Super-Kamiokande I–IV. *Phys. Rev. D* **2018**, *97*, 072001. [CrossRef]
15. Li, Z.; et al. [Super-Kamiokande Collaboration]. Measurement of the tau neutrino cross section in atmospheric neutrino oscillations with Super-Kamiokande. *Phys. Rev. D* **2018**, *98*, 052006. [CrossRef]
16. Renshaw, A.; et al. [Super-Kamiokande Collaboration]. First Indication of Terrestrial Matter Effects on Solar Neutrino Oscillation. *Phys. Rev. Lett.* **2014**, *112*, 091805. [CrossRef] [PubMed]
17. Abe, K.; et al. [Super-Kamiokande Collaboration]. Solar neutrino measurements in Super-Kamiokande-IV. *Phys. Rev. D* **2016**, *94*, 052010. [CrossRef]
18. Zhang H.; et al. [Super-Kamiokande Collaboration]. Supernova Relic Neutrino search with neutron tagging at Super-Kamiokande-IV. *Astropart. Phys.* **2015**, *60*, 41–46. [CrossRef]
19. Abe, K.; et al. [Super-Kamiokande Collaboration]. Search for proton decay via $p \to e^+\pi^0$ and $p \to \mu^+\pi^0$ in 0.31 megaton·years exposure of the Super-Kamiokande water Cherenkov detector. *Phys. Rev. D* **2017**, *95*, 012004. [CrossRef]

20. Abe, K.; et al. [Super-Kamiokande Collaboration]. Search for nucleon decay into charged antilepton plus meson in 0.316 megaton·years exposure of the Super-Kamiokande water Cherenkov detector. *Phys. Rev. D* **2017**, *96*, 012003. [CrossRef]
21. Press, W.H.; Spergel, D.N. Capture by the sun of a galactic population of weakly interacting, massive particles. *Astrophys. J.* **1985**, *296*, 679–684. [CrossRef]
22. Joseph, S.; Keith, O.; Mark, S. The photino, the sun, and high-energy neutrinos. *Phys. Rev. Lett.* **1985**, *55*, 257.
23. Gaisser, T.K.; Steigman, G.; Tilav, S. Limits on cold-dark-matter candidates from deep underground detectors. *Phys. Rev. D* **1986**, *34*, 2206. [CrossRef]
24. Andrew, G. Resonant enhancements in weakly interacting massive particle capture by the earth. *Astrophys. J.* **1987**, *321*, 571–585.
25. John, E.; Enqvist, K.; Nanopoulous, D.V.; Tamvakis, K. Gaugino masses and grand unification. *Phys. Lett. B* **1985**, *155*, 381–386.
26. Bottino, A.; Fornengo, N.; Scopel, S. Light relic neutralinos. *Phys. Rev. D.* **2003**, *67*, 063519. [CrossRef]
27. Niro, V.; Bottino, A.; Fornengo, N.; Scopel, S. Investigating light neutralinos at neutrino telescopes. *Phys. Rev. D* **2009**, *80*, 095019. [CrossRef]
28. Kaustubh, A.; Yanou, C.; Lina, N.; Jesse, T. (In)direct detection of boosted dark matter. *Cosmol. Astropart. Phys.* **2014**, *10*, 62.
29. Huang, J.; Zhao, Y. Dark matter induced nucleon decay: Model and signatures. *J. High Energy Phys.* **2014**, *2014*, 77. [CrossRef]
30. Cherry, J.F.; Frandsen, M.T.; Shoemaker, I.M. Direct Detection Phenomenology in Models Where the Products of Dark Matter Annihilation Interact with Nuclei. *Phys. Rev. Lett.* **2015**, *114*, 231303. [CrossRef]
31. Kachulis, C.; et al. [Super-Kamiokande Collaboration]. Search for Boosted Dark Matter Interacting with Electrons in Super-Kamiokande. *Phys. Rev. Lett.* **2018**, *120*, 0221301. [CrossRef] [PubMed]
32. Choi, K.; et al. [Super-Kamiokande Collaboration]. Search for Neutrinos from Annihilation of Captured Low-Mass Dark Matter Particles in the Sun by Super-Kamiokande. *Phys. Rev. Lett.* **2014**, *114*, 141301.
33. Abe, K.; et al. [Super-Kamiokande Collaboration]. Limits on sterile neutrino mixing using atmospheric neutrinos in Super-Kamiokande. *Phys. Rev. D* **2015**, *91*, 052019. [CrossRef]
34. Abe, K.; et al. [Super-Kamiokande Collaboration]. Test of Lorentz invariance with atmospheric neutrinos. *Phys. Rev. D* **2015**, *91*, 052003. [CrossRef]
35. Super-Kamiokande Web Page. Available online: http://www-sk.icrr.u-tokyo.ac.jp/sk/publications/index-e.html (accessed on 9 January 2019).
36. Sanuki, T.; Honda, M.; Kajita, T.; Kasahara, K.; Midorikawa, S. Study of cosmic ray interaction model based on atmospheric muons for the neutrino flux calculation. *Phys. Rev. D* **2007**, *75*, 043005. [CrossRef]
37. Honda, M.; Kajita, T.; Kasahara, K.; Midorikawa, S.; Sanuki, T. Calculation of atmospheric neutrino flux using the interaction model calibrated with atmospheric muon data. *Phys. Rev. D* **2007**, *75*, 043006. [CrossRef]
38. Honda, M.; Kajita, T.; Kasahara, K.; Midorikawa, S. Improvement of low energy atmospheric neutrino flux calculation using the JAM nuclear interaction model. *Phys. Rev. D* **2011**, *83*, 123001. [CrossRef]
39. Honda, M.; Sajjad, A.M.; Kajita, T.; Kasahara, K.; Midorikawa, S. Atmospheric neutrino flux calculation using the NRLMSISE-00 atmospheric model. *Phys. Rev. D* **2015**, *92*, 023004. [CrossRef]
40. Bernabeu, J.; Palomares-Ruiz, S.; Petcov, S.T. Atmospheric neutrino oscillations, θ_{13} and neutrino mass hierarchy. *Nucl. Phys. B* **2003**, *669*, 255–276. [CrossRef]
41. Chizhov, M.; Maris, M.; Petcov, S.T. On the Oscillation Length Resonance in the Transitions of Solar and Atmospheric Neutrinos Crossing the Earth Core. *arXiv* **1998**, arXiv:hep-ph/9810501.
42. Akhmedov, E.K.; Dighe, A.; Lipari, P.; Smirnov, A.Y. Atmospheric neutrinos at super-Kamiokande and parametric resonance in neutrino oscillations. *Nucl. Phys. B* **1999**, *542*, 3–30. [CrossRef]
43. Peres, O.L.G.; Smirnov, A.Y. Atmospheric neutrinos: LMA oscillations, Ue3 induced interference and CP-violation. *Nucl. Phys. B* **2004**, *680*, 479–509. [CrossRef]
44. Olive, K.A.; et al. [Particle Data Group]. Review of Particle Physics. *Chin. Phys. C* **2014**, *38*, 090001. [CrossRef]
45. Abe, K.; et al. [T2K Collaboration]. Combined Analysis of Neutrino and Antineutrino Oscillations at T2K. *Phys. Rev. Lett.* **2017**, *118*, 0151801. [CrossRef] [PubMed]
46. Abe, K.; et al. [T2K Collaboration]. Measurements of neutrino oscillation in appearance and disappearance channels by the T2K experiment with 6.6×10^{20} protons on target. *Phys. Rev. D* **2015**, *118*, 072010.

47. Adamson, P.; et al. [NOvA Collaboration]. Measurement of the Neutrino Mixing Angle θ_{23} in NOvA. *Phys. Rev. Lett.* **2017**, *118*, 151802. [CrossRef] [PubMed]
48. Aartsen, M.G.; Abraham, K.; Ackermann, M.; Adams, J.; Aguilar, J.A.; Ahlers, M.; Altmann, D.; Anderson, T.; Ansseau, I.; Archinger, M.; et al. Neutrino oscillation studies with IceCube-DeepCore. *Nucl. Phys. B* **2016**, *908*, 161–177. [CrossRef]
49. Adamson, P.; et al. [MINOS Collaboration]. Combined Analysis of ν_μ Disappearance and $\nu_\mu \rightarrow \nu_e$ Appearance in MINOS Using Accelerator and Atmospheric Neutrinos. *Phys. Rev. Lett.* **2014**, *112*, 191801. [CrossRef]
50. Martin, A.D.; Ryskin, M.G.; Stasto, A.M. Prompt neutrinos from atmospheric c-cbar and b-bbar production and the gluon at very small x. *Acta Phys. Pol. B* **2003**, *34*, 3273–3304.
51. Abe, K.; et al. [Super-Kamiokande Collaboration]. Evidence for the Appearance of Atmospheric Tau Neutrinos in Super-Kamiokande. *Phys. Rev. Lett.* **2013**, *110*, 181803.
52. Kodama, K.; et al. [DONuT Collaboration]. Final tau-neutrino results from the DONuT experiment. *Phys. Rev. D* **2008**, *78*, 052002. [CrossRef]
53. Agafonova, N.; et al. [OPERA Collaboration]. Final Results of the OPERA Experiment on ν_τ Appearance in the CNGS Neutrino Beam. *Phys. Rev. Lett.* **2018**, *120*, 211801. [CrossRef] [PubMed]
54. Philipp, E.; Feifei, H.; Michael, L. Measurement of Atmospheric Tau Neutrino Appearance with IceCube/DeepCore. In Proceedings of theNEUTRINO2018– XXVIII International Conference on Neutrino Physics and Astrophysics, Heidelberg, Germany, 4–10 June 2018.
55. Bahcall John, N.; Ulrich Roger, K. Solar models, neutrino experiments, and helioseismology. *Rev. Mod. Phys.* **1988**, *60*, 297. [CrossRef]
56. Cleveland, B.T.; Daily, T.; Davis, R., Jr.; Distel, J.R.; Lande, K.; Lee, C.K.; Wildenhain, P.S.; Ullman, J. Measurement of the Solar Electron Neutrino Flux with the Homestake Chlorine Detector. *Astrophys. J.* **1998**, *496*, 505–526. [CrossRef]
57. Abdurashitov, J.N.; et al. [SAGE Collaboration]. Measurement of the solar neutrino capture rate with gallium metal. III. Results for the 2002–2007 data-taking period. *Phys. Rev. C* **2009**, *80*, 015807. [CrossRef]
58. Fukuda, Y.; et al. [Kamiokande Collaboration]. Solar Neutrino Data Covering Solar Cycle 22. *Phys. Rev. Lett.* **1996**, *77*, 1683. [CrossRef] [PubMed]
59. Ahmad, Q.R.; et al. [SNO Collaboration]. Direct Evidence for Neutrino Flavor Transformation from Neutral-Current Interactions in the Sudbury Neutrino Observatory. *Phys. Rev. Lett.* **2002**, *89*, 011301. [CrossRef]
60. Bellini, G.; et al. [Borexino Collaboration]. Final results of Borexino Phase-I on low-energy solar neutrino spectroscopy. *Phys. Rev. D* **2014**, *89*, 112007. [CrossRef]
61. Gando, A.; et al. [KamLAND Collaboration]. ^{7}Be solar neutrino measurement with KamLAND. *Phys. Rev. C* **2015**, *92*, 055808. [CrossRef]
62. Fkuda, S.; et al. [Super-Kamiokande Collaboration]. Solar ^{8}B and hep Neutrino Measurements from 1258 Days of Super-Kamiokande Data. *Phys. Rev. Lett.* **2001**, *86*, 5651. [CrossRef]
63. Ahmad, Q.R.; et al. [SNO Collaboration]. Measurement of the Rate of $\nu_e + d \rightarrow p + p + e^-$ Interactions Produced by ^{8}B Solar Neutrinos at the Sudbury Neutrino Observatory. *Phys. Rev. Lett.* **2001**, *87*, 071301. [CrossRef]
64. Smirnov, A.Y. Solar neutrinos: Oscillations or No-oscillations? *arXiv* **2016**, arXiv:1609:02386.
65. De Holanda, P.C.; Smirnov, A.Y. Homestake result, sterile neutrinos, and low energy solar neutrino experiments. *Phys. Rev. D* **2004**, *69*, 113002. [CrossRef]
66. De Holanda, P.C.; Smirnov, A.Y. Solar neutrino spectrum, sterile neutrinos, and additional radiation in the Universe. *Phys. Rev. D* **2011**, *83*, 113011. [CrossRef]
67. Barger, V.; Patrick, H.; Danny, M. Solar Mass-Varying Neutrino Oscillations. *Phys. Rev. Lett.* **2005**, *95*, 211802. [CrossRef] [PubMed]
68. Friedland, A.; Lunardini, C.; Pena-Garay, C. Solar neutrinos as probes of neutrino–matter interactions. *Phys. Lett. B* **2004**, *594*, 347–354. [CrossRef]
69. Miranda, O.G.; Tórtola, M.A.; Valle, J.W. Are solar neutrino oscillations robust? *J. High Energy Phys.* **2006**, *10*, 008. [CrossRef]
70. Nakahata, M.; et al. [Super-Kamiokande Collaboration]. Calibration of Super-Kamiokande using an electron LINAC. *Nucl. Instrum. Methods A* **1999**, *421*, 113–129. [CrossRef]

71. Blaufuss, E.; et al. [Super-Kamiokande Collaboration]. ^{16}N as a calibration source for Super-Kamiokande. *Nucl. Instrum. Methods A* **2001**, *458*, 638–649. [CrossRef]
72. Hosaka, J.; et al. [Super-Kamiokande Collaboration]. Solar neutrino measurements in Super-Kamiokande-I. *Phys. Rev. D* **2006**, *73*, 112001. [CrossRef]
73. Cravens, J.P.; et al. [Super-Kamiokande Collaboration]. Solar neutrino measurements in Super-Kamiokande-II. *Phys. Rev. D* **2008**, *78*, 032002. [CrossRef]
74. Abe K.; et al. [Super-Kamiokande Collaboration]. Solar neutrino results in Super-Kamiokande-III. *Phys. Rev. D* **2011**, *83*, 052010. [CrossRef]
75. Aharmim, B.; et al. [SNO Collaboration]. Combined analysis of all three phases of solar neutrino data from the Sudbury Neutrino Observatory. *Phys. Rev. C* **2013**, *88*, 025501. [CrossRef]
76. Source: WDC-SILSO, Royal Observatory of Belgium, Brussels. Available online: http://www.sidc.be/silso/datafiles (accessed on 9 January 2019).
77. Nakano, Y.; Sekiya, H.; Tasaka, S.; Takeuchi, Y.; Wendell, R.A.; Matsubara, M.; Nakahata, M. Measurement of radon concentration in Super-Kamiokande's buffer gas. *Nucl. Instrum. Methods A* **2017**, *867*, 108–114. [CrossRef]
78. Nakano, Y. Radon background study in Super-Kamiokande. *J. Phys. Conf. Ser.* **2017**, *888*, 012191. [CrossRef]
79. Nakano, Y. ^{8}B Solar Neutrino Spectrum Measurement Using Super-Kamiokande IV. Ph.D. Thesis, The University of Tokyo, Tokyo, Japan, 2016. Available online: http://www-sk.icrr.u-tokyo.ac.jp/sk/_pdf/articles/2016/doc_thesis_naknao.pdf (accessed on 9 January 2019).
80. Agostini, M.; et al. [Borexino Collaboration]. First Simultaneous Precision Spectroscopy of pp, ^{7}Be, and pep Solar Neutrinos with Borexino Phase-II. *arXiv* **2017**, arXiv:1707:09279.
81. Gando, A.; et al. [KamLAND Collaboration]. Reactor on-off antineutrino measurement with KamLAND. *Phys. Rev. D* **2013**, *88*, 033001. [CrossRef]
82. An, F.P.; et al. [Daya Bay Collaboration]. Improved measurement of electron antineutrino disappearance at Daya Bay. *Chin. Phys. C* **2013**, *37*, 011001. [CrossRef]
83. Ahn, J.K.; et al. [RENO Collaboration]. Observation of Reactor Electron Antineutrinos Disappearance in the RENO Experiment. *Phys. Rev. Lett.* **2012**, *108*, 191802. [CrossRef]
84. Abe, Y.; et al. [Double Chooz Collaboration]. Reactor $\bar{\nu}_e$ disappearance in the Double Chooz experiment. *Phys. Rev. D* **2012**, *86*, 052008. [CrossRef]
85. Ken'ichiro, N.; Eri, M.; Yuu, N.; Hideyuki, S. Spectrum of the supernova relic neutrino background and metallicity evolution of galaxies. *Astrophys. J.* **2015**, *804*, 75.
86. Horiuchi, S.; Beacom, J.F.; Dwek, E. Diffuse supernova neutrino background is detectable in Super-Kamiokande. *Phys. Rev. D* **2009**, *79*, 083013. [CrossRef]
87. Bays K.; et al. [Super-Kamiokande Collaboration]. Supernova relic neutrino search at Super-Kamiokande. *Phys. Rev. D* **2012**, *85*, 052007. [CrossRef]
88. Watanabe, H.; et al. [Super-Kamiokande Collaboration]. First study of neutron tagging with a water Cherenkov detector. *Astropart. Phys.* **2009**, *31*, 320–328. [CrossRef]
89. Beacom John, F.; Vargins Mark, R. Antineutrino Spectroscopy with Large Water Čerenkov Detectors. *Phys. Rev. Lett.* **2004**, *93*, 171101. [CrossRef] [PubMed]